Enhancing the Lubricity and Wear Resistance of Shape-Memory-Polymer via Titanium Carbide-based MAX and MXene

Shubham Jaiswal[1,2], Jeet Vishwakarma[1,2], Shubham Bhatt[3], Reuben J. Yeo[4], Rahul Mishra[3], Chetna Dhand[1,2,*], Neeraj Dwivedi[1,2,*]

[1]CSIR-Advanced Materials and Processes Research Institute, Bhopal- 462026, India

[2]Academy of Scientific and Innovative Research (AcSIR), Ghaziabad- 201002, India

[3]Centre for Applied Research in Electronics, Indian Institute of Technology Delhi, New Delhi 110016, India

[4]Institute of Materials Research and Engineering (IMRE), Agency for Science, Technology, and Research (A*STAR), 2 Fusionopolis Way, Innovis #08-03, Singapore 138634, Singapore

Corresponding Authors

[*] **Email:** chetna.dhand@ampri.res.in **and** chetnachem24@gmail.com (C. Dhand)

[*] **Email:** neeraj.dwivedi@ampri.res.in **and** neerajdwivedi6@gmail.com (N. Dwivedi)

Keywords: Smart composites, MAX and MXene, Sliding friction and wear

Abstract

Sliding surfaces not only consume an exceptional amount of energy to overcome friction but also cause premature failure of mechanical systems due to wear, leading them to be frequently replaced. Friction and wear are, therefore, major concerns from the viewpoints of energy consumption, cost, and the environment. Here we report for the first time the development of tribologically resilient and self-healing smart composites comprising shape-memory polyurethane (SMPU) as the model polymer matrix and titanium carbide-based MAX and MXene materials as fillers. The ball-on-disk tribological tests and 3D optical surface profilometry tests are performed to examine the coefficient of friction and wear. The introduction of layered MAX and MXene phase materials exceptionally reduces the friction of SMPU by 2-3 times and reduces its wear rate by 2-3 orders of magnitude, even at low filler concentrations of 0.25 wt%. In-depth wear track analysis, using Raman spectroscopy and EDAX elemental mapping, reveals the presence of MAX and MXene at the wear track, in addition to tribochemically formed TiO_2, which contributes to the SMPU's lubricity and wear resistance. Furthermore, the developed materials reveal damage healing capability, which is not hindered by the reinforcement of MAX and MXene as well. The results suggest that by using these composites, not only the friction and wear but also the frequent replacement of sliding components can be minimized, which is crucial for cost-saving and environmentally sustainable technologies.

Introduction

When surfaces in contact slide against each other, friction is generated, which could lead to wear of the materials. High friction and wear are, therefore, major concerns in mechanical components with moving parts. These tribological interactions account for about 23% (119 EJ) of all energy consumed worldwide. About 20% (103 EJ) of this energy is used to reduce friction, and around 3% (16 EJ) is used to remanufacture worn components and spare equipment as a result of wear and wear-related failures[1]. Thus, even a minor reduction of friction and wear is of huge importance as it could lead to significant energy and cost savings.

To alleviate this friction and wear concerns, manufacturing more wear-resistant and lubricious composites or surface modification of the components by plasma treatment, ion bombardment, and coating are among the most commonly used practices [2-4]. In particular, composites of metals, ceramics, and polymers have shown exceptional tribological behavior due to the synergistic interaction between the different filler and matrix materials that results in the reinforcement of the composite [5-10]. Recently, polymer materials have been largely sought for their tribological applications as they are lightweight, corrosion-resistant, low-cost, and can be engineered relatively tough compared to metallic materials. In addition, some engineered polymer materials possess advantageous friction and wear characteristics coupled with self-lubrication, suitable viscoelasticity, and heat resistance, which make them well-suited for high-speed machinery applications such as those being used in aerospace engineering, hydropower plants, and the automotive sector. The reinforcement by foreign material fillers such as carbon nanotubes, graphene, graphene oxide, metal chalcogenides, and metal/ceramic nanomaterials has been used to further boost the tribological characteristics of the polymeric materials [11-15], and the search for novel high-performance fillers for this purpose is still ongoing.

MAX phase materials are layered ternary carbide or nitride, comprising an early transition metal element "M", a group 3A or group 4A element in the periodic table denoted as “A”, and either carbon or nitrogen denoted as "X". MXene is produced by etching the “A” layer from a MAX phase material, giving a lamellar material with the general formula of $M_{n+1}X_n$, where n has a value of 1, 2 or 3[16-20]. MAX and MXene materials offer some unique advantages as fillers for composites compared to other 2D materials like graphene and transition metal dichalcogenides (TMDCs). MAX phases, which serve as MXene precursors, have a nifty blend of metallic and ceramic properties, making them capable of boosting both electrical and thermal conductivities and mechanical strength in composites [18, 21]. MXenes, in general, have a hydrophilic nature, making them bond well with the matrix materials and solve filler dispersion issues seen with many other 2D materials[22]. In the tribological aspect, MXenes' unique combination of properties, including their layered structure, low shear strength, good thermal conductivity, and high mechanical robustness, holds promise for improving wear resistance and frictional performance in composite materials [23, 24]. With a wide array of compositions and the ability to fine-tune properties by varying elements, MXenes open the possibilities for versatile, and customized composites. Due to its astonishing functional properties, MXene as a reinforcing phase in polymer composite materials is under intense investigation for various applications [25, 26]. In particular, for tribological applications, the tribological properties of pristine MXene coating [27], and composite coatings comprising MXene and other 2D materials [28] have been studied. The $Ti_3C_2T_x$ MXene (where T_x represents functional groups) is known for its outstanding tribological [23, 29] and mechanical characteristics due to its layered structure and surface terminations. These features weaken the interlayer coupling, reduce the shear strength through decreased binding energies, and ultimately cause a decrease in frictional force [30, 31]. Moreover, a few reports on the tribology of MXene-reinforced polymer composites also exist. For example, Zhang *et al.* [32]

enhanced the surface hardness and anti-friction performance of an ultrahigh-molecular weight polyethylene matrix by Ti_3C_2 MXene reinforcement. The researchers predicted that the improved friction and wear performance of polymer-MXene composites is attributed to their enhanced mechanical properties and their capability to form tribo-films that help to reduce direct contact of the material with the counterface [33]. In another example, the tribological performance of a V_2C MXene-polyacrylic acid composite coating has also been investigated [34]. However, in general, the mechano-tribological aspects of MXene-reinforced composites are not well understood. We also hypothesize that the parent MAX phase materials may be used as fillers to enhance significantly the tribological characteristics of polymer composites due to the presence of the carbide phases in MAX phase materials. However, to the best of our knowledge, no such research has been reported so far.

When traditional tribological components have been subjected to excessive wear and tear, they are frequently replaced. This not only raises the issue of waste accumulation and environmental pollution but also increases the maintenance cost of the equipment due to part replacement. Moreover, the onset of microscopic cracks or defects in the component could lead to catastrophic failure if not detected early. Like most biomaterials/biosystems with an intrinsic ability to self-heal or self-repair, developing self-repairable yet tribological resilient materials/systems could be a game changer. This would minimize the downtime of the machine, material waste, the cumulative replacement costs of the component, and the likelihood of catastrophic machine failure if the damage or crack in the component can be instantly repaired upon its onset. The self-healing capability of intelligent materials has recently been shown to vastly improve the lifetime, safety, and reliability of materials in various applications [35-38]. Some examples of smart materials include shape memory polymers (SMPs) and their composites, which could be promising in this regard.

In this work, we report the development of intelligent SMP composites containing MAX and MXene filler materials to simultaneously realize tribological composite materials with low friction, high wear resistance, and self-repair capability.

Results

To develop tribologically resilient intelligent composites, we used shape memory polyurethane (SMPU) as the model matrix and Ti_3C_2 (MXene), Ti_2AlC (MAX_1), and Ti_3AlC_2 (MAX_2) materials as the fillers. The SMPU is referred to as PU hereafter. Before the development of composites, we first thoroughly characterized the starting MAX and MXene phase materials. X-ray diffraction (XRD) patterns (Figure 1a) revealed the typical <002> peak of the MAX and MXene phases along with the signature of higher d-spacing in MXene than MAX phase materials [20]. The MAX_1 exhibits a <002> peak at 13.85°, suggesting a d-spacing of 0.64 nm and a c-parameter of 1.3 nm, while showing a small <002> peak related to Ti_3AlC_2, indicating mixed phases. MAX_2 (Ti_3AlC_2) displays a <002> peak at 9.3°, indicating a d-spacing of 0.95 nm and a c-parameter of 1.90 nm. Regarding MXene, its <002> peak appears at approximately 8.9°, revealing an interlayer spacing of about 0.99 nm (close to the typical reported value of 1 nm) with a c-parameter of 1.98 nm [20]. The absence of <104> peaks in MXene shows that the Al layer was successfully etched away from its precursor Ti_3AlC_2 MAX phase. Many other reflections corresponding to Ti_2AlC/Ti_3AlC_2 MAX and Ti_3C_2 MXene phases with some impurities were also observed (Figure 1a). Further, Raman spectra (Figure 1b) for MAX_1 and MAX_2 displayed a peak at ~143 cm^{-1} corresponding to the E_{2g} vibration mode. Additionally, two peaks at 260 cm^{-1} and 600 cm^{-1} in MAX_1 and a peak at 600 cm^{-1} in MAX_2 can be attributed to the overlapping vibrations of the E_{2g} and E_{1g} modes [39]. Whereas the peak at 260 cm^{-1} in MAX_2 corresponds to A_{1g} out-of-plane symmetric vibrations. On the other hand, in Ti_3C_2

MXene, distinct peaks are observed at 210 cm^{-1} and 700 cm^{-1} (Figure 1b). These peaks are assigned to A_{1g} vibrations of the (Ti, O, C) and (C-C) bonds, respectively. Peaks at 370 cm^{-1} and 610 cm^{-1} for Ti_3C_2 are associated with in-plane (E_g) vibration modes of the O_2 group attached to Ti atoms, where the latter peak mainly originates from E_g vibration modes of the carbon atoms in OH-terminated Ti_3C_2[40]. Consequently, the XRD and Raman analyses confirm the presence of the Ti_3C_2 MXene phase in MXene, Ti_3AlC_2 MAX phase in MAX_2, and a mixture of Ti_2AlC and Ti_3AlC_2 MAX phases in MAX_1. Further, the MAX_1, MAX_2, and MXene morphologies were examined using a field emission scanning electron microscope (FESEM), revealing the presence of flakes and layer structures (Figure 1c) [20]. To get further insight into the microstructure of MAX and MXene phase materials, high-resolution transmission electron microscopy (HRTEM) measurements were performed on Ti_3AlC_2 (MAX_2) and Ti_3C_2 (MXene) materials, Figure 1d. The HRTEM images show the typical layered structure of Ti_3AlC_2 (MAX_2) and Ti_3C_2 (MXene) with interlayer spacing of 0.95 nm and 1.02 nm, respectively, corroborating the XRD results. X-ray photoelectron spectroscopy (XPS) was performed to understand further the chemical composition and bonding within the MAX and MXene phase fillers. Figure 1e shows the deconvoluted C 1s and Ti 2p spectra and high-resolution Al 2p spectra for MAX_1, MAX_2, and MXene samples. The C 1s spectra (Figure 1e) of MAX_1 and MAX_2 were fitted with three peaks (C_1 to C_3), whereas an additional C_4 peak was required to fit the C 1s spectrum of MXene. In all three MAX and MXene samples, the strongest peak C_1 corresponds to Ti-C bonding, whereas peaks C_2 and C_3 correspond to sp^2 C (graphite or graphene-like) and sp^3C (including C-H) bonding, respectively, which is consistent with literature[41-43]. The additional peak C_4 in MXene corresponds to C-O bonding, suggesting the presence of oxygen-containing groups.

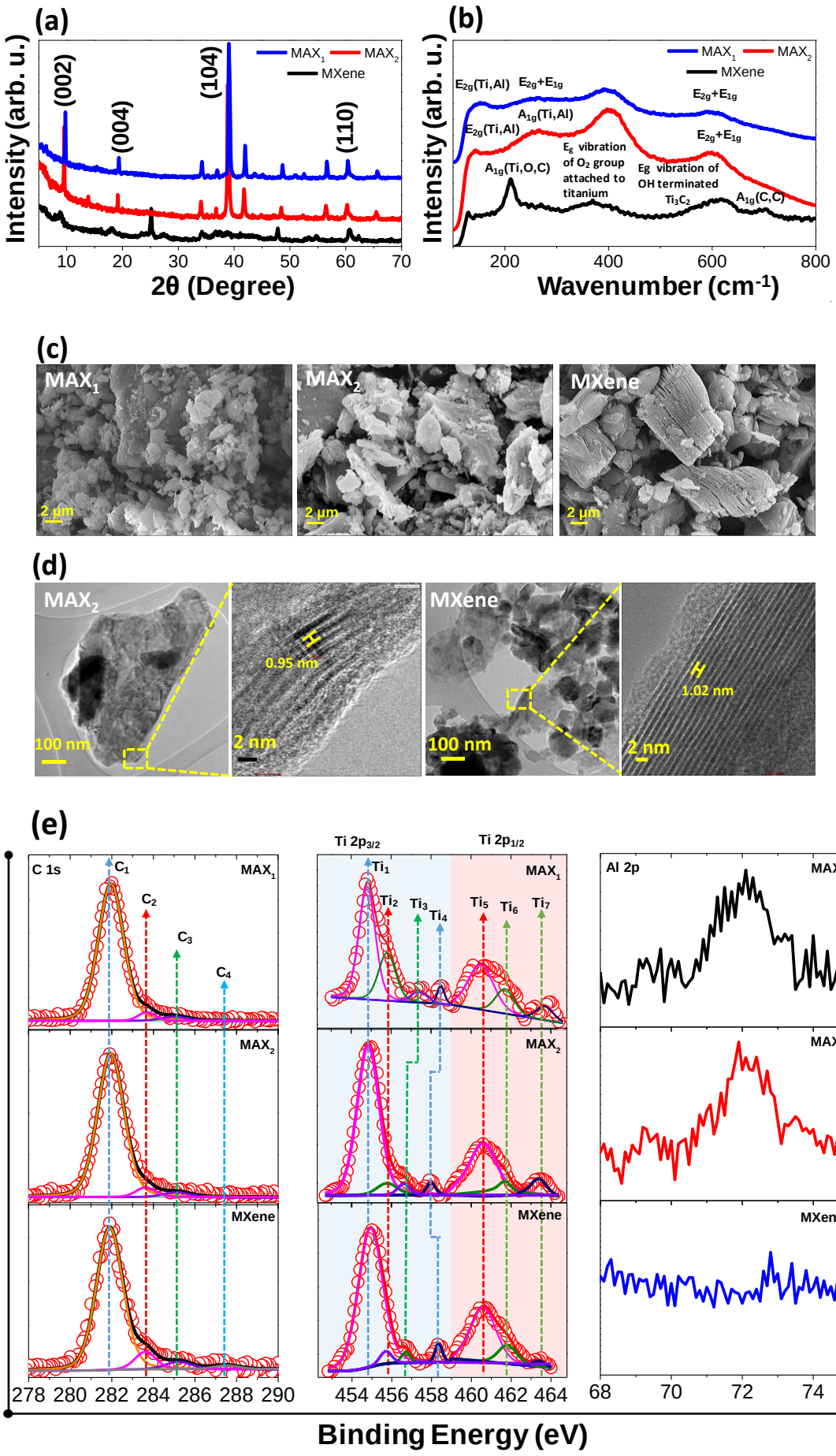
(a)
Intensity (arb. u.)
(002)
(004)
(104)
(110)
MAX1
MAX2
MXene
10 20 30 40 50 60 70
2θ (Degree)
(b)
Intensity (arb. u.)
MAX1
MAX2
MXene
E2g(Ti,Al)
E2g+E1g
A1g(Ti,Al)
A1g(Ti,O,C)
Eg vibration of O2 group attached to titanium
Eg vibration of OH terminated Ti3C2
A1g(C,C)
200 400 600 800
Wavenumber (cm-1)
(c)
MAX1
MAX2
MXene
2 μm
(d)
MAX2
100 nm
0.95 nm
2 nm
MXene
100 nm
1.02 nm
2 nm
(e)
Intensity (arb. u.)
C 1s
C1
C2
C3
C4
MAX1
MAX2
MXene
278 280 282 284 286 288 290
Ti 2p3/2
Ti 2p1/2
Ti1
Ti2
Ti3
Ti4
Ti5
Ti6
Ti7
MAX1
MAX2
MXene
454 456 458 460 462 464
Al 2p
MAX1
MAX2
MXene
68 70 72 74
Binding Energy (eV)

Figure 1: Characterization of starting MAX and MXene phase materials. (a) X-ray Diffraction (XRD) analysis illustrating the crystallographic structures and phase purity of MAX_1, MAX_2, and MXene materials. (b) Raman spectroscopy depicting the vibrational modes and structural changes in MAX_1, MAX_2, and MXene phases. (c) FESEM images provide surface morphology details and microstructural characteristics of MAX_1, MAX_2, and MXene samples. (d) HRTEM micrographs showcasing the nanoscale morphology lattice interlayer spacing within MAX_2, and MXene phases. (e) X-ray Photoelectron Spectroscopy (XPS) measurements elucidating the elemental composition, chemical states, and surface properties of MAX_1, MAX_2, and MXene phase materials.

Generally, the C 1s region is easily influenced by carbon-containing contaminants when the sample is exposed to the ambient environment. However, unlike a pure-carbon system such as amorphous carbon, diamond, graphite, etc., which reveals a C 1s peak close to the adventitious carbon peak (284.5-285.0 eV) [44-46], we are studying metal carbide MAX and MXene (Ti_3C_2 and Ti_3AlC_2). In the C 1s spectra, the titanium carbide peak (Ti-C) appears around 282.0 eV. Hence, the binding energy separation between the Ti-C peak and adventitious carbon peak is significantly large (about 2.8-3 eV) and they can be distinguished as different peaks. Moreover, we found a very intense 282.0 eV peak in the XPS C 1s spectra and very weak C_2 and C_3 peaks. Thus, the XPS C 1s spectra are dominated by peak C_1 corresponding to Ti-C bonding [47]. This suggests that the signal arising from carbon contamination from the environment is very low in these samples. Nonetheless, the tail of peak C_2 and the starting region of peak C_3 (range close to 284.8-285 eV) may have some contribution from adventitious carbon along with sp^2C and sp^3C bonding, respectively.

To further understand the bonding characteristics, the Ti 2p XPS spectra were analyzed. The Ti 2p spectra comprised a doublet peak of Ti $2p_{3/2}$ and Ti $2p_{1/2}$, due to spin-orbital coupling [48], Figure 1e. The Ti $2p_{3/2}$ and Ti $2p_{1/2}$ envelops complemented the C 1s spectra, with the most substantial Ti_1 (in Ti $2p_{3/2}$) and Ti_5 (in Ti $2p_{1/2}$) peaks being assigned to Ti-C bonding that is present in the MAX and MXene samples[42]. Adjacent to the Ti_1 peak, the Ti_2 peak, also present in all the samples, was assigned to Ti-C/C-Ti^{2+} (O/OH) bonding [41-43, 49]. On the

other hand, the comparatively weaker Ti_3 and Ti_4 peaks were assigned to the bonding of Ti with O, *i.e.,* Ti-O bonding [43]. Likewise, in the Ti $2p_{1/2}$ envelop, peak Ti_6 corresponds to Ti-C/C-Ti^{2+} (O/OH) bonding whereas peak Ti_7 represents Ti-O bonding. Further, the Al 2p spectra recorded for these samples revealed the absence of a peak in MXene. For the MAX_1 and MAX_2 samples, the Al peak was found to be broadened, corresponding to Al-O/OH bonding. The presence of O/OH-related bonding peaks in the C 1s, Ti 2p, and Al 2p spectra is attributed to atmospheric impurities. However, the MXene sample may have acquired O/OH groups during chemical etching of the "A" layer of the MAX phase.

PU-composites were prepared using a micro-compounder technique [50] to introduce MAX_1, MAX_2, and MXene fillers into the PU matrix. Filler concentrations of 0.25 wt.%, 0.5 wt.%, 1.0 wt.%, and 2.0 wt.% for each type of filler were investigated in this work (***see*** **Experimental Section** for detailed experimental methods). The sliding friction and wear properties of the PU composites were evaluated using a ball-on-disk tribometer. The representative coefficient of friction (COF) curves for pristine PU, PU-MAX_1, PU-MAX_2, and PU-MXene composites are shown in Figures 2a-c. From these curves, the average COF for each sample was derived based on at least 4-5 test repetitions (Figure 2d). At first glance, the introduction of MAX and MXene was shown to largely reduce the COF of PU (Figure 2a-c). For instance, the average COF of pristine PU (~0.35) was significantly reduced to < 0.13 in the PU composites, indicating that the introduction of the fillers contributed to a reduction in the COF by up to three times (Figure 2d). From Figures 2a-c, we initially witnessed smooth sliding on PU as the tribological measurement began. However, with continued cycling, the COF of PU increased after 700 cycles. We hypothesize that as the number of cycles increased, the contact area significantly altered due to frictional heat, causing the deformation, and the onset of major adhesive and abrasive wear. These collectively contributed to the increase of COF after 700 cycles. The calculated values of percentage reduction in the average COF for

the PU-composites samples, with respect to pristine PU, are shown in Figure 2e. The data clearly reveal the large reduction of COF (> 50%) with the introduction of the MAX and MXene fillers. Interestingly, the extent of friction alteration was not considerably changed with the increase of MAX and MXene loading from 0.25 wt.% to 2.0 wt.%, suggesting that even a small amount of reinforcement of 0.25 wt.% was sufficient to immensely reduce and stabilize the friction of PU. Further, optical images of the wear track and the counterface ball after the ball-on-disk tribological tests reveal the severe wear of pristine PU after sliding, as evident from the broad and intense wear track formed on the sample and the large amount of debris transferred from the PU sample to the ball (Figure 3a and/or Figure S1a). However, the reinforcement of PU by MAX and MXene phase materials significantly reduced the wear of PU, as confirmed by the observation of relatively narrower and shallower wear tracks on the PU-composites samples, as well as substantially less debris transfer to the balls (*See* **supplementary Note 1**). Further, we have also summarized some of the interesting works on different layered or 2D materials as fillers for polymer matrices (Table 1), including shape memory polymers, and compared their tribological performance with the current work having MAX and MXene as fillers for shape memory polyurethane. The comparison reveals that the MAX and MXene hold great promise as fillers to control the tribological properties of polymeric materials.

Table 1: Comparison of different 2D/layered materials as fillers for different polymer matrices to control the tribological properties.

Modal matrix	**Filler**	**Reduct-ion in COF (%)**	**Reduct-ion in wear (%)**	**Testing Parameters**			**Refer-ences**
				Test setup	**Counter-face material**	**Conditi-ons**	
Polyphenylene sulfide (PPS)/polytetra fluoroethylene	WS_2@ Ti_3C_2 nanoh ybrid	----	59.3%	Pin-on-Disk	AISI-1045 steel	2 mm diameter , 35–55 MPa,	[51]

(PTFE) fabric composites						0.4 m/s, 2 hours	
Epoxy (EP) resin	WS_2@ GO	47.04%	36.57%	Ball-on-Disk	304 steel ball	6 mm diameter, 10 N load, 200 r/min rotation speed	[15]
Ultra-High Molecular Weight Polyethylene (UHMWPE)	WS_2	61.1	-----	Ball-on-Disk	Si_3N_4 ball	Reciprocating motion (10 mm distance, 1 Hz), 10 N load, 1800 s, under water lubrication	[52]
Poly(vinyl butyral) (PVB)	Inorganic fullerene-like (IF-WS_2)	48%.	----	Berkovich Indentation	Diamond tip	3-sided pyramidal tip (142.35° included angle, 65.35° half-angle), loading: 10 s, hold: 15 s, unloading: 5 s, 1 mN force. Nanoscratch: 5 s ramping force, 15 s at 1 mN and 0.66 mm/s,	[53]

						return, 5 s unload	
Epoxy (EP)	CNF/ MoS_2 hybrid	82%	86%	Ball-on-Disk	440c ball	8mm diameter, load: 3N-6N, speed: 100-400 rpm/min, 20 minutes	[54]
Ultra-High Molecular Weight Polyethylene (UHMWPE)	fluorinated graphene	27%	43%	Ball-on-Disk	Zirconia ceramic ball	5.0 N load, 1 hour, 10 mm/s sliding speed, 3 Hz frequency, 6.56 MPa contact pressure	[55]
Nomex fabric/phenolic composite	PS-graphene	9%	19%	Pin-on-Disk	AISI-1045 pin	2 mm diameter, dry sliding, room temp, 94-251 N, 0.28-0.73 m/s, 2 hours	[56]
Shape memory polyimide (SMPI)	modified boron nitride	~38%	88.9%	Pin-on-Disk	GCr15 steel ball	Dry sliding under air, 20 N load, 200 r/min, 5 mm radius, 1800 s, 188.50 m distance	[57]

Shape memory polyurethane (SMPU)	Ti_2AlC (MAX_1)/Ti_3AlC_2(MAX_2)/Ti_3C_2 (MXene)	~62.8%	~99-99.8%	Ball-on-Disk	Stainless steel (100 Cr 6)	2 mm diameter ball, 100 rpm rotation, 1.0 N load, 6000 cycles, 30°C, RH 30±5%	This work

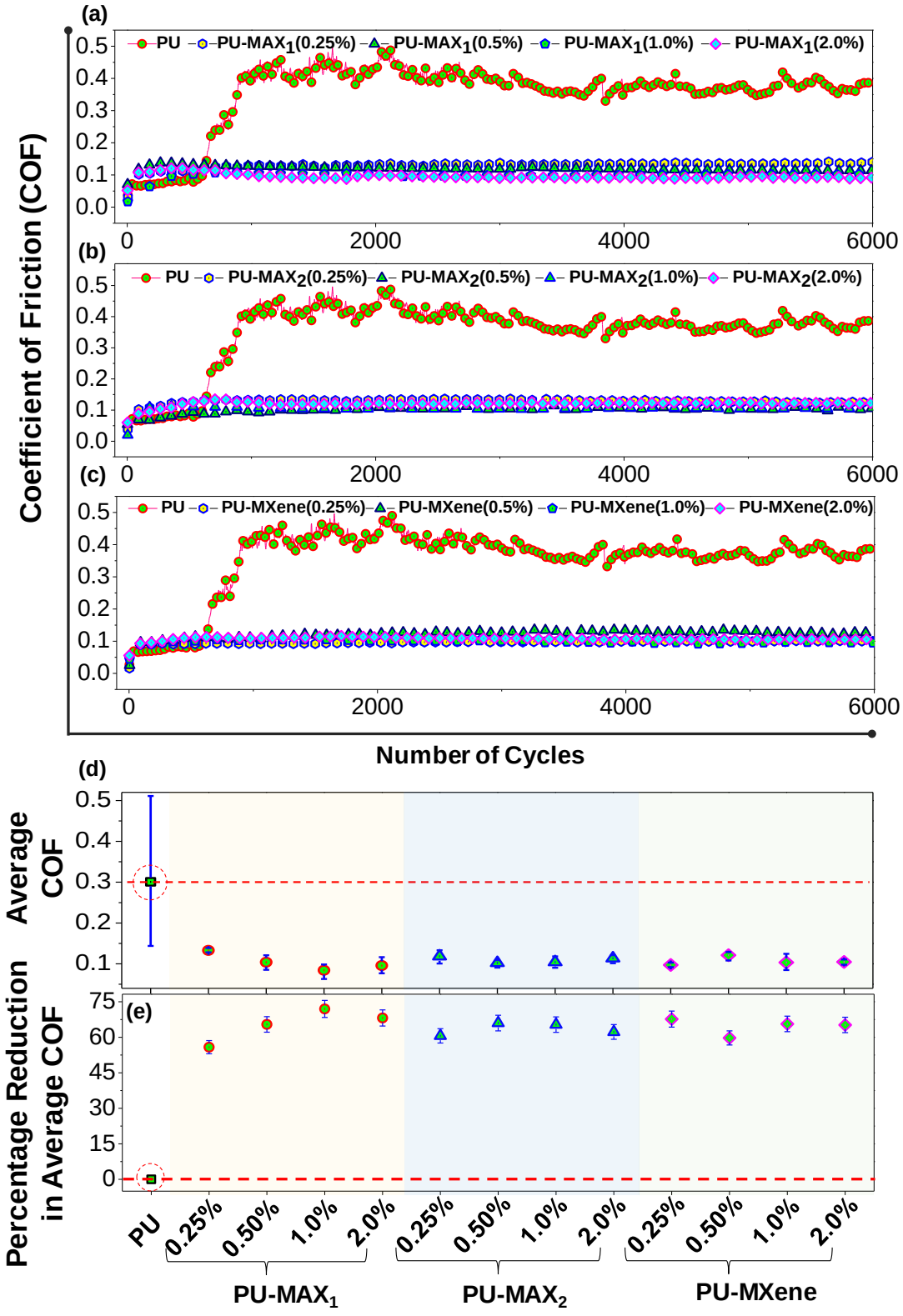

Figure 2: (a-c) Frictional curves of (a) PU-MAX_1, (b) PU-MAX_2, and (c) PU-MXene composites; the reference frictional curve of pristine PU is shown in (a)-(c) for comparison purposes. (d) Average COF values of pristine PU and PU-composites samples extracted from steady-state friction region (viz. 1000-6000 cycles) of the tribological tests; the average COF value for each sample was determined from at least 4-5 tribological tests at different locations

on the same sample. (e) Percentage reduction in the average COF of the PU-composites with respect to pristine PU.

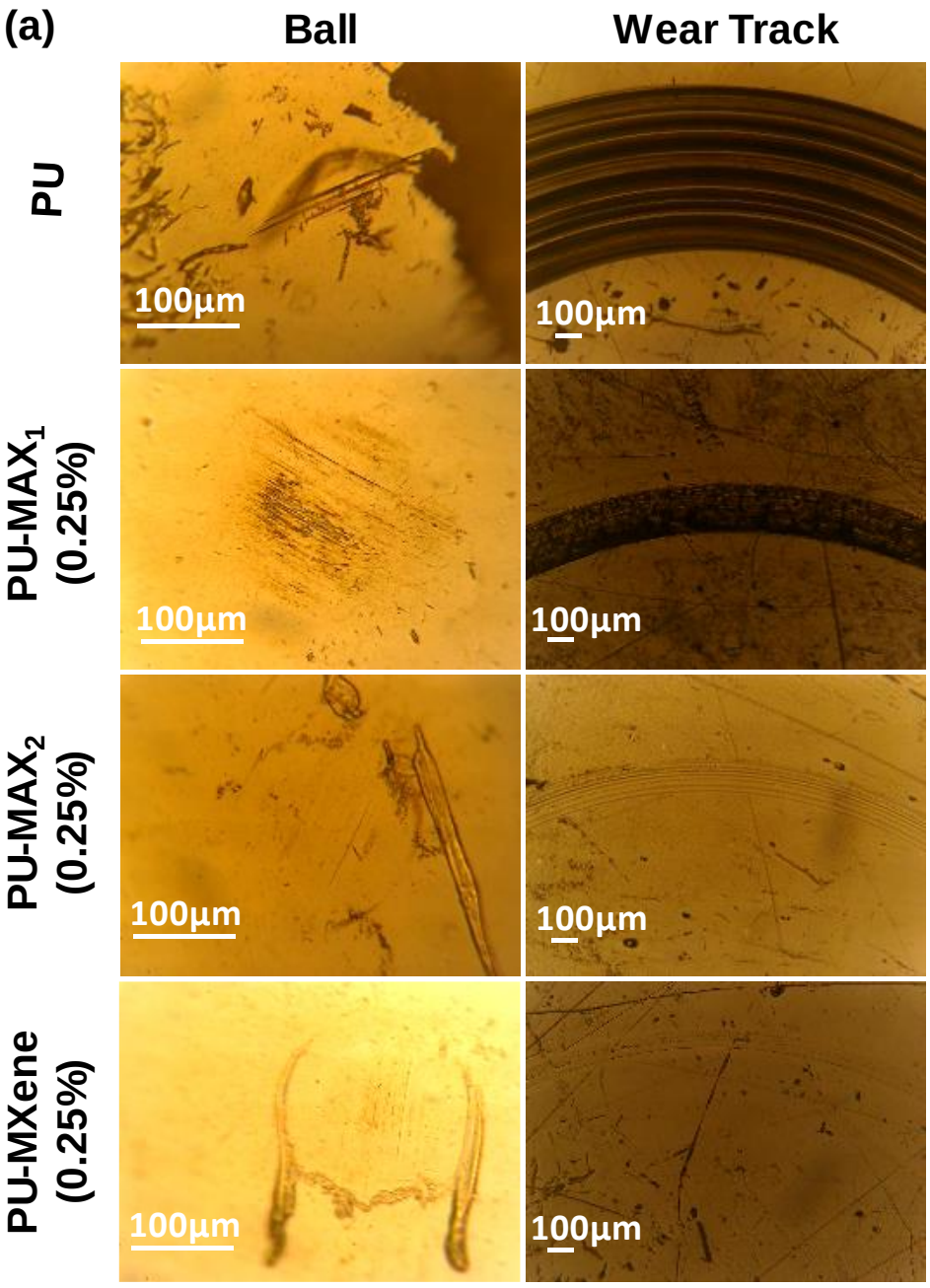

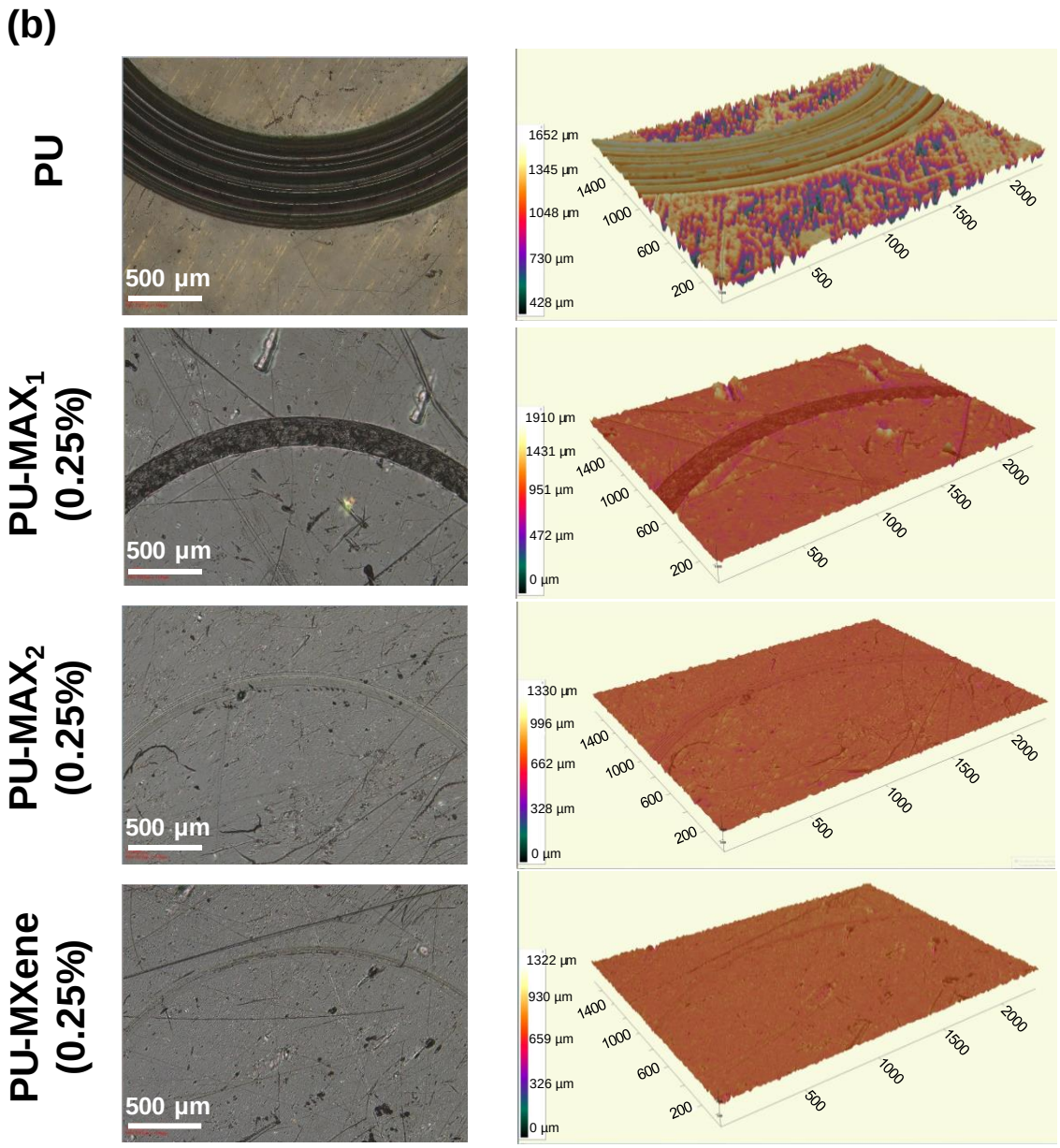

Figure 3: Optical images and 3D surface profiles of pristine PU, PU-MAX_1, PU-MAX_2, and PU-MXene composites with a filler concentration of 0.25 wt. % after tribological measurements. (a) Optical microscope images of the wear tracks and counter-face balls captured after the tribological tests. (b) The 2D (left column) and 3D (right column) optical surface profiles of the wear tracks, illustrating the differences in wear track depths.

The detailed analysis of the samples' surface properties, wear tracks' characteristics, and elemental composition is crucial to discovering and understanding the friction and wear mechanisms that take place during sliding. 3D optical surface profilometry measurements were carried out to examine the wear tracks' profiles and quantify the wear rates of selected samples.

Figure 3b shows the 2D and 3D wear track images recorded using an optical surface profilometer. The wear rate of each sample was quantitatively analyzed based on the wear depth measured from the 3D wear track images. The pristine PU sample showed a substantially higher wear rate of $2 \times 10^{-2}\ mm^3N^{-1}m^{-1}$ than the PU-MAX_1 (0.25 wt.%), PU-MAX_2 (0.25 wt.%), and PU-MXene (0.25 wt.%) composites samples, which displayed wear rates of 4.3×10^{-4}, 2×10^{-4}, and $4 \times 10^{-5}\ mm^3N^{-1}m^{-1}$, respectively. This corresponds to 50 times, 100 times, and 500 times enhancement in the wear resistance of PU after the introduction of 0.25 wt. % of MAX_1, MAX_2, and MXene fillers each, respectively. It is thus evident from the wear rate data that, as a filler material for PU, the Ti_3C_2 MXene phase material is superior to MAX phase material for tribological applications. From the 3D optical profilometer images, the surface roughnesses of the samples were also measured (Figure S2). The surface roughness of pristine PU was much higher than the MAX and MXene-reinforced PU-composite samples (See **supplementary Note 2**). We predict that the introduction of MAX and MXene facilitated the shearing and good mixing of the PU-composites during the sample preparation stage compared to pristine PU, which contributed to making the surface flatter and smoother. Furthermore, Raman spectroscopy (Figure 4a) and energy dispersive X-ray analysis (EDAX) (Figure S1b) measurements were performed to investigate the chemical composition of the wear tracks. The Raman spectra were recorded across various locations on the wear track (locations L1 to L4), as visualized by the corresponding optical microscope images, for pristine PU and PU reinforced with 2.0 wt.% of MAX_1, MAX_2, and MXene. The Raman spectra of wear tracks for PU-composites show few peaks that could correspond to MAX/MXene or related materials. Closer examination of the spectra reveals a few more TiO_2 bands (anatase phase) at ~ 400 cm^{-1} (B_{1g}) and 639 cm^{-1} (E_g), likely of tribo-chemical origin, in addition to the previously observed E_g band at ~140 cm^{-1} [58]. Additionally, elemental mapping of the wear tracks was performed using EDAX. Figure S1b shows the SEM images of the wear track

location where EDAX mapping was performed for each sample, as well as the EDAX maps of selected elements (**See Supplementary Note 1**). However, because the wear of the PU-composites is significantly lower than pristine PU, the wear track impression could not be observed in Ti, Al, C, and O elemental imaging for PU-composite samples. Overall, elemental maps of the PU-composites clearly reveal the traces of constituent elements of MAX/MXene and PU such as Ti, Al, C, and O on the wear track, which suggest that the MAX and MXene fillers were present at the sliding interfaces and likely played an important role in facilitating the low friction contact sliding.

Discussion

It is observed that the application of both MAX and MXene-phase materials extraordinarily reduces the sliding friction and wear of PU. The extent of friction reduction reaches nearly 63%, and wear resistance increases by about 2 orders of magnitude for PU-composites compared to pristine PU. The COF strongly depends on the shear strength, *i.e.*, a low shear strength of a material in direct contact with the sliding counterface causes the two bodies to easily slide across each other with reduced COF. The tribological tests on the PU-composites can be described by the tribosystems of a steel/PU-MAX composite pair or a steel/PU-MXene composite pair. Conversely, in the absence of the fillers, the tribosystem for the tribological test on pristine PU can be described by a simple steel/PU pair. MAX and MXene materials are interesting because they possess characteristics of metals and ceramics and have a layered structure composed of a stack of multiple layers akin to many other 2D materials. Thus, when one of the components of the tribo-pair starts to slide against the other, high shear stresses are generated at the tribo-interface, which propagate and facilitate shear/exfoliation of the layered MAX and MXene containing PU due to decreased shear strength. Hence, the low and stable friction observed in PU-composites compared to pristine PU. Furthermore, it was also observed

that the application of MAX and MXene reduces the plastic deformation (*see* **Supplementary Note 3**), which could reduce the plastic contact area and contribute to lower friction of PU-composites. In addition, the lower surface roughness of PU-composites compared to pristine PU (Figure S2) could assist in reducing the friction barrier and lowering the COF in PU-composites.

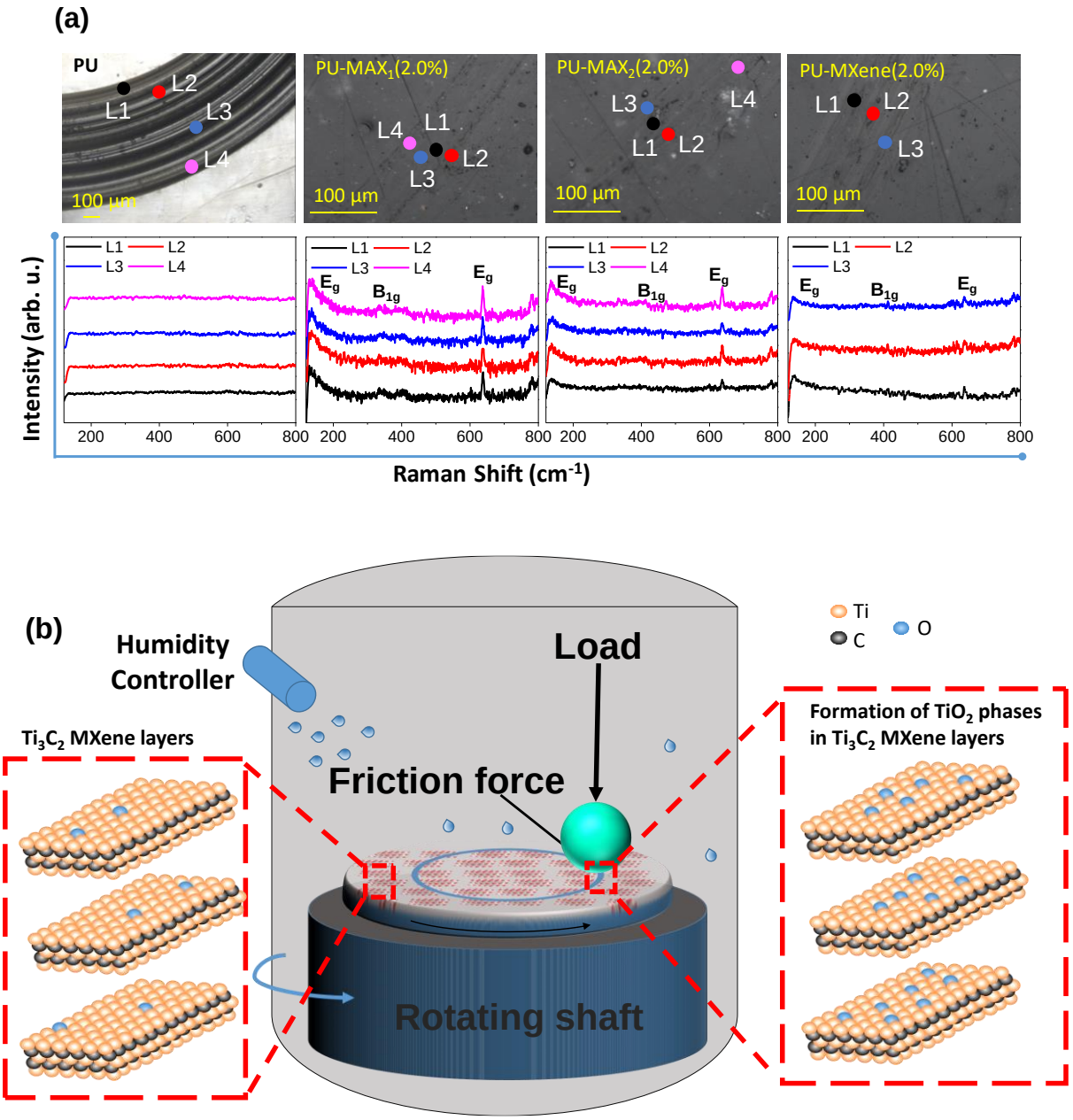

Figure 4: (a) Optical microscope images (top) and Raman spectra (bottom) taken at various locations on the wear tracks (labeled L1 to L4) to confirm the presence of the constituent elements; (b) Scheme illustrating the sliding of composites against the ball (steel) and

occurrence of tribo-chemical reaction to generate more TiO_2 phases which facilitate lubricious and wear resistance properties of composites in a tested environment.

Finally, tribological heating is another critical issue that could negatively affect the tribological behavior of a polymer, especially for polymers with low thermal conductivity. Since the MAX and MXene fillers contribute to a higher thermal conductivity of the PU-composites than that of pristine PU (*see* **Supplementary Note 4**), the heat generated by friction during contact sliding could be transferred more rapidly through the PU-composites, which may have prevented shape deformation of the polymeric sample as well as contact area alteration that might otherwise occur due to overheating of the sample. Thus, the higher thermal conductivity of the PU-composites may have also led to their lower friction. Further, the surface roughness also considerably affects the friction and wear of the materials. A low surface roughness causes the system to slide with low friction and reduces resistance to wear[59]. Hence, reduced roughness of PU-composites due to MAX and MXene reinforcements contribute to their low friction and wear, compared to pristine PU.

To understand why MAX and MXene-filled PU composites maintain lower friction throughout the tribological tests, wear track analysis was performed. Previously, wear track analysis using EDAX revealed the presence of constituent Ti, C, and Al atoms of MAX/MXene along with O (**Supplementary Note 2**). By performing Raman spectroscopy at various locations across each wear track region, we noticed the occurrence of tribochemical reactions at sliding interfaces of PU-MAX and PU-MXene composites (Figure 4a). This led to the formation of additional TiO_2 peaks (Anatase phase) on the wear track as a consequence of tribochemical oxidation of Ti in MAX and MXene. Thus, the amount of TiO_2 phase materials enhances on the wear track. It is known that the reinforcement properties contributed by TiO_2 particles can improve the tribological properties such as friction and wear of polymers [60]. Hence the layered MAX/MXene materials, together with TiO_2, both facilitate the low friction

sliding in PU-composites. Also, the presence of MAX/MXene and their related materials, such as TiO_2, on the wear tracks helps to maintain lower friction and wear of the PU-composites throughout the test. We have schematically illustrated the sliding of the MXene-filled PU composite against the steel ball in the ball-on-disk tribological test and the partial tribochemical conversion of MXene to TiO_2 on the wear track that also contributes to lower and stable friction throughout the test (Figure 4b) [32, 61]. On the other hand, the enhanced wear resistance of PU-composites could also be attributed to better mechanical properties (such as hardness) of MAX, and MXene [62, 63] than pristine PU, the higher mechanical strength of the TiO_2 phase compared to PU, reduced deformation, and low friction-induced reduction in wear.

The self-healing capabilities of the samples (Figures 5a-5e) were tested by intentionally introducing a dent into the samples' surfaces. The dent was created by applying a load of ~400N to the sample surface using a universal tensile machine. Figures 5d-e show the optical images of the intentionally dented samples before (Figure 5d) and after healing (Figure 5e). The supplementary movie **SM-1** also demonstrates the damage-repairing capability of the samples. Figures 5d-5e and SM-1 clearly show that pristine PU demonstrates damage healing ability, which remains maintained in PU-composites reinforced with 0.25 wt.% of MAX_1, MAX_2, and MXene fillers. The healing mechanism is explained in schematic diagrams shown in Figures 5a-c. The self-healing mechanism in physically crosslinked PU can be attributed to the abundance of reversible physical crosslinks and thermo-reversible bonds, as well as the ease of diffusion of the polymer chains in PU. PU is typically composed of polymer chains interconnected by reversible physical crosslinks, which can deform/break and re-form when the material changes temperature or when other external stimuli (such as heat energy, electrical energy, etc.) are applied. On the application of external force/pressure, the PU gets deformed due to the breaking of crosslinks, allowing the polymer chains to move freely. The crosslinks re-form as the materials are exposed to external stimuli, enabling the material to revert to its

original shape. The polymer chains in physically crosslinked PU can diffuse and flow, allowing the material to heal small cracks or damages. The healing ability of PU also relies on thermo-reversible bonds, such as hydrogen bonds or van der Waals forces, to hold the polymer chains together. These bonds can break and re-form under mild heating, facilitating healing. It is important to note that the self-healing ability of physically crosslinked PU is typically effective for small-scale damage or reversible deformation.

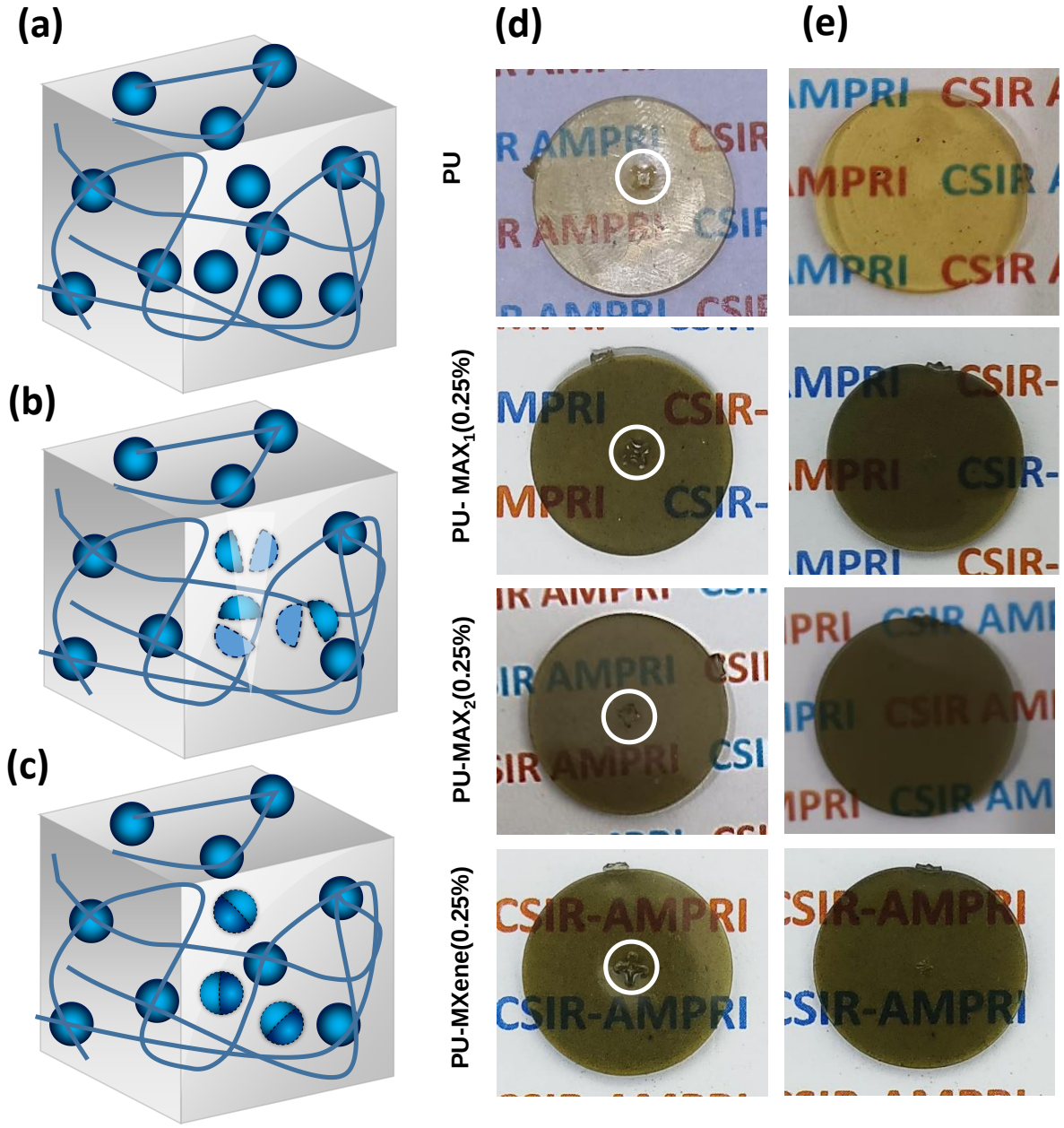

Figure 5: (a)-(c) Schematic diagram to show the working mechanism of self-healing in PU and PU-composites; in figure (b), the dotted structures represent the deformed/broken segments of PU, whereas figure (c) shows healing of those segments upon their exposure to external stimulus. (d & e) Photographs of pristine PU and PU-MAX_1, PU-MAX_2, and PU-MXene composites with a filler concentration of 0.25 wt.%, from top to bottom, showing (d) the samples just after the creation of a dent (as indicated by the white circle) and (e) the samples after self-healing. The dent was formed by applying a load of ~400 N onto the samples' surfaces using a universal testing machine.

Further examination of the tensile properties of these samples (***see*** **Supplementary Note 3**) indicates that 0.25 wt. % of MAX and MXene-based fillers are adequate for achieving

improved tensile strength properties with marginal elongation degradation. It was also observed that introducing MAX and MXene phase fillers reduces the plastic deformation.

Conclusions

PU-composites containing 0.25, 0.5, 1.0, and 2.0 wt.% of Ti_2AlC (MAX_1), Ti_3AlC_2 (MAX_2), and Ti_3C_2 (MXene) were successfully prepared *via* conventional melt mixing techniques. Tribological ball-on-disk sliding tests showed that the developed PU composites possessed significantly better contact sliding properties than pristine PU. Our detailed studies revealed that the reinforcement provided by even a small amount of these fillers in PU (0.25 wt%) resulted in 2-3 times lower COFs and ~2-3 orders of magnitude lower wear rates than pristine PU. An in-depth investigation of the wear tracks revealed the tribochemical formation of TiO_2, which is also famous for its lubricious nature and excellent mechanical properties as a filler material in polymer composites. Additionally, the PU-composites reinforced with just 0.25 wt.% MAX and MXene phase materials also maintain self-healing properties. Overall, MAX and MXenes are promising filler materials that can exceptionally boost the tribological characteristics of SMPs. This is pivotal for enabling next-generation intelligent materials in industrial applications.

Experimental Methods

Materials: PU granules (ether type) were used as the starting SMP matrix material. Three different types of transition metal carbides (MAX and MXene phases), namely Ti_2AlC (MAX_1) (≤ 40 μm), Ti_3AlC_2 (MAX_2) (≤ 40 μm), and Ti_3C_2 (MXene) (≤ 40 μm) were used as the fillers.

Synthesis of PU-composites: The PU-composite samples were prepared through the melt mixing of PU with MAX_1, MAX_2, and MXene. The resultant samples are denoted as PU-

MAX_1, PU-MAX_2, and PU-MXene. The mixture of PU with different MAX and MXene phase materials was first melt-blended in a twin-screw micro-compounder (Thermo Haake micro-compounder MiniLab 3), and the pellets were then collected in an injecting cylinder for injection molding (Thermo Scientific HAAKE MiniJet Pro Piston). Disk and dumbbell-shaped samples were prepared where the MAX_1, MAX_2, and MXene filler concentrations varied from 0.25 wt.% to 2.0 wt.%. Thus, a total of 13 different types of compositions were prepared, namely: pristine PU, PU-MAX_1 (0.25%), PU-MAX_1 (0.5%), PU-MAX_1 (1%), PU-MAX_1 (2%), PU-MAX_2 (0.25%), PU-MAX_2 (0.5%), PU-MAX_2 (1%), PU-MAX_2 (2%), PU-MXene (0.25%), PU-MXene (0.5%), PU-MXene (1%) and PU-MXene (2%).

Characterizations of the materials and PU-composites: The MAX_1, MAX_2, and MXene filler materials and all fabricated PU-composites were characterized using a range of microscopic and spectroscopic tools. XRD measurements were carried out using Rigaku MiniFlex and X'Pert PRO diffractometers with Cu K_α radiation ($\lambda = 0.15418$ nm) using a 2θ angle range from 5^o to 60^o. Raman measurements (Airix Corporation, Japan) were performed at a laser wavelength of 514 nm. The laser power and the acquisition time were optimized to get a reasonable signal-to-noise ratio. The morphologies of MAX and MXene phase materials were monitored using FESEM (ZEISS ULTRA plus) tool. HRTEM measurements (TALOS 200kV S-FEG, FEI) were performed at an accelerating voltage of 200KV to investigate the morphological/structural properties of MAX and MXene phase materials. Using the Al Kα beam as the source of radiation (*hv* = 1486.6 eV), the XPS (*PHI Quantera SXM Scanning X-ray Microprobe*) measurements were performed to examine the bonding states of MAX and MXene phase material. The beam's spot size of 200 μm × 200 μm was used for all the samples.

Likewise, for core-level XPS spectra the pass energy and step size were kept to be 55 eV and 0.1 eV, respectively. Tribological measurements were performed on pristine PU and PU-

composites using a ball-on-disk low load tribometer (DUCOM Instruments) under controlled conditions (Temperature 30 °C and Relative Humidity of $30 \pm 5\%$). A stainless steel (100 Cr 6) ball 2 mm in diameter was used as the counterface. All tests were carried out in rotating disk mode, with a circular track diameter of 2 mm and a rotation speed of 100 rpm. The ball applied a constant normal load of 1.0 N on the sample throughout the test, and the coefficient of friction was measured for 6000 cycles (revolutions). The maximum Hertzian contact pressure was also calculated and found to be 21 MPa. After each test, images of the steel ball and the sample surface where the test had been conducted were captured using a microscope equipped with a digital camera to observe the extent of wear. The wear rate was estimated using the following formula:

$$W = \frac{V}{S \times F} \qquad (1)$$

where S is the sliding length (m), F is the applied normal load (N), and V is the wear volume (mm^3). The wear volume V is obtained by measuring the depth and width of the wear track using a 3D optical profilometer (MicroXAM-100, KLA-Tencor Corporation, USA). This is a non-contact, non-destructive optical technique used to measure the sample's surface topography, including surface roughness, surface waviness, and step heights, with the capability of 2-dimensional and 3-dimensional imaging.

To investigate the chemical states of MAX and MXene phase materials after the tribological tests on the PU-composite samples, Micro-Raman measurements (Airix Corporation, Japan) were performed at various locations on the wear tracks using a laser wavelength of 514.5 nm with optimized acquisition time and laser power. Furthermore, SEM-EDS (Jeol JCM-7000) was employed for elemental mapping of the wear tracks. The mechanical properties of pristine PU and PU-composites, such as ultimate tensile stress, elongation at break, toughness, and elastic modulus, were estimated from uniaxial tensile tests using Tinius and Olsen H25KT

universal testing machines. The tensile tests were performed on the dumbbell-shaped samples (ISO 527-2 die standards) with a gauge length of 30 mm and strain rate of 20 mm/min. The tests were performed 10-12 times to ensure the repeatability of the results.

Furthermore, water contact angle measurements (KRUSS drop Analyzer) were performed to study the surface wettability of pristine PU and PU-composites. Freshly prepared DI water drops, 10 microlitres each, were dispensed onto the surfaces of pristine PU and PU-composite samples. The contact angles were estimated from the images of the drops on the surfaces with a side-view CCD camera. Water contact angle measurements (***see*** **Supplementary Note 5**) indicate that reinforcement of MAX and MXene slightly altered the surface wettability of PU. However, the trend for contact angle was noticed to be irregular with tuning of the concentration of MAX and MXene phase fillers.

Acknowledgments

The authors thank the Director Council of Scientific and Industrial Research (CSIR)-Advanced Materials and Processes Research Institute (AMPRI), India, for his kind support. The Council of Scientific and Industrial Research (CSIR), India, supports this research through the MLP 303 project. S. J. acknowledges CSIR, India, for providing financial support through the JRF/SRF fellowship. The authors wish to thank Dr. Pradip Kumar, Dr. Rajeev Kumar, Dr. D. P. Mondal, Dr. P. Asokan, Dr. M. Shafeeq M., Mr. D. K. Kashyap, Mr. A. Khare, Mr. N. Prashant, and Dr A. Naik from CSIR-Advanced Materials and Processes Research Institute, Bhopal, India for their help. The authors also wish to thank Dr. Pratima Solanki and Dr. Amit Kumar Yadav from Jawahar Lal Nehru University, New Delhi, for their support.

Authors Contribution

N. D. conceived the idea. N. D. and S. J. designed the project. S. J. prepared the samples and performed the characterizations. J. V., N. D., S. B., R. J. Y., R. M., and C. D. helped in characterizations. N. D., J. V., S. B., R. J. Y., R. M., and C. D. provided constructive inputs on experimental results analysis. S. J. wrote the initial draft of the manuscript. All the authors critically reviewed the manuscript and helped to improve the manuscript draft.

Conflict of Interest

The authors declare no conflict of interest

Data Availability Statement

The data that support the findings of this study are available at reasonable request from the corresponding author.

References

[1] K. Holmberg, A. Erdemir, Influence of tribology on global energy consumption, costs and emissions, Friction 5(3) (2017) 263-284.
[2] X. Zeng, Y. Peng, H. Lang, A novel approach to decrease friction of graphene, Carbon 118 (2017) 233-240.
[3] M. Parvinzadeh, I. Ebrahimi, Atmospheric air-plasma treatment of polyester fiber to improve the performance of nanoemulsion silicone, Applied Surface Science 257(9) (2011) 4062-4068.
[4] K.Y. Rhee, S.J. Park, D. Hui, Y. Qiu, Effect of oxygen plasma-treated carbon fibers on the tribological behavior of oil-absorbed carbon/epoxy woven composites, Composites Part B: Engineering 43(5) (2012) 2395-2399.
[5] W.X. Chen, J.P. Tu, L.Y. Wang, H.Y. Gan, Z.D. Xu, X.B. Zhang, Tribological application of carbon nanotubes in a metal-based composite coating and composites, Carbon 41(2) (2003) 215-222.
[6] E. Omrani, A. Dorri Moghadam, P.L. Menezes, P.K. Rohatgi, New Emerging Self-lubricating Metal Matrix Composites for Tribological Applications, in: J.P. Davim (Ed.), Ecotribology: Research Developments, Springer International Publishing, Cham, 2016, pp. 63-103.
[7] T. Rodriguez-Suarez, J.F. Bartolomé, J.S. Moya, Mechanical and tribological properties of ceramic/metal composites: A review of phenomena spanning from the nanometer to the micrometer length scale, Journal of the European Ceramic Society 32(15) (2012) 3887-3898.
[8] J. Mohapatra, S. Nayak, M.M. Mahapatra, Mechanical and tribology properties of Al-4.5%Cu-5%TiC metal matrix composites for light-weight structures, International Journal of Lightweight Materials and Manufacture 3(2) (2020) 120-126.

[9] J. Tian, X. Qi, C. Li, G. Xian, Friction behaviors and wear mechanisms of multi-filler reinforced epoxy composites under dry and wet conditions: Effects of loads, sliding speeds, temperatures, water lubrication, Tribology International 179 (2023) 108148.
[10] S. Kumar, K.K. Singh, Tribological characteristics of glass/carbon fibre-reinforced thermosetting polymer composites: a critical review, Journal of the Brazilian Society of Mechanical Sciences and Engineering 44(11) (2022) 496.
[11] P.H.V. Soares, P.N. de Oliveira, C.C. Viáfara, G.G. Silva, L.G. Amurin, A.B. da Silva, Effect of the reduced graphene oxide on the tribological behavior of UHMWPE/rGO nanocomposites under sliding contact conditions, Polymer Engineering & Science 62(8) (2022) 2641-2656.
[12] F. Li, K.-a. Hu, J.-l. Li, B.-y. Zhao, The friction and wear characteristics of nanometer ZnO filled polytetrafluoroethylene, Wear 249(10) (2001) 877-882.
[13] M.S. Sreekala, C. Eger, Property Improvements of an Epoxy Resin by Nanosilica Particle Reinforcement, in: K. Friedrich, S. Fakirov, Z. Zhang (Eds.), Polymer Composites: From Nano- to Macro-Scale, Springer US, Boston, MA, 2005, pp. 91-105.
[14] Y. Li, S. Wang, E. He, Q. Wang, The effect of sliding velocity on the tribological properties of polymer/carbon nanotube composites, Carbon 106 (2016) 106-109.
[15] Y. Li, Y. Zhou, Y. Wang, M. Liu, J. Yuan, X. Men, Facile synthesis of WS2@GO nanohybrids for significant improvement in mechanical and tribological performance of EP composites, Tribology International 163 (2021) 107148.
[16] M. Naguib, V.N. Mochalin, M.W. Barsoum, Y. Gogotsi, 25th Anniversary Article: MXenes: A New Family of Two-Dimensional Materials, Advanced Materials 26(7) (2014) 992-1005.
[17] M. Alhabeb, K. Maleski, B. Anasori, P. Lelyukh, L. Clark, S. Sin, Y. Gogotsi, Guidelines for Synthesis and Processing of Two-Dimensional Titanium Carbide (Ti3C2Tx MXene), Chemistry of Materials 29(18) (2017) 7633-7644.
[18] M. Aakyiir, H. Yu, S. Araby, W. Ruoyu, A. Michelmore, Q. Meng, D. Losic, N.R. Choudhury, J. Ma, Electrically and thermally conductive elastomer by using MXene nanosheets with interface modification, Chemical Engineering Journal 397 (2020) 125439.
[19] M. Naguib, M. Kurtoglu, V. Presser, J. Lu, J. Niu, M. Heon, L. Hultman, Y. Gogotsi, M.W. Barsoum, Two-Dimensional Nanocrystals Produced by Exfoliation of Ti3AlC2, Advanced Materials 23(37) (2011) 4248-4253.
[20] M. Naguib, O. Mashtalir, J. Carle, V. Presser, J. Lu, L. Hultman, Y. Gogotsi, M.W. Barsoum, Two-Dimensional Transition Metal Carbides, ACS Nano 6(2) (2012) 1322-1331.
[21] B. Anasori, M.R. Lukatskaya, Y. Gogotsi, 2D metal carbides and nitrides (MXenes) for energy storage, Nature Reviews Materials 2(2) (2017) 1-17.
[22] Y.-Z. Zhang, J.K. El-Demellawi, Q. Jiang, G. Ge, H. Liang, K. Lee, X. Dong, H.N. Alshareef, MXene hydrogels: fundamentals and applications, Chemical Society Reviews 49(20) (2020) 7229-7251.
[23] M. Malaki, R.S. Varma, Mechanotribological Aspects of MXene-Reinforced Nanocomposites, Advanced Materials 32(38) (2020) 2003154.
[24] M. Chhattal, A. Rosenkranz, S. Zaki, K. Ren, A. Ghaffar, Z. Gong, P.G. Grützmacher, Unveiling the tribological potential of MXenes-current understanding and future perspectives, Advances in Colloid and Interface Science 321 (2023) 103021.
[25] H. Wei, J. Dong, X. Fang, W. Zheng, Y. Sun, Y. Qian, Z. Jiang, Y. Huang, Ti3C2Tx MXene/polyaniline (PANI) sandwich intercalation structure composites constructed for microwave absorption, Composites Science and Technology 169 (2019) 52-59.
[26] M. Cai, H. Yan, Y. Li, W. Li, H. Li, X. Fan, M. Zhu, Ti3C2Tx/PANI composites with tunable conductivity towards anticorrosion application, Chemical Engineering Journal 410 (2021) 128310.
[27] P.G. Grützmacher, S. Suarez, A. Tolosa, C. Gachot, G. Song, B. Wang, V. Presser, F. Mücklich, B. Anasori, A. Rosenkranz, Superior Wear-Resistance of Ti3C2Tx Multilayer Coatings, ACS Nano 15(5) (2021) 8216-8224.
[28] S. Huang, K.C. Mutyala, A.V. Sumant, V.N. Mochalin, Achieving superlubricity with 2D transition metal carbides (MXenes) and MXene/graphene coatings, Materials Today Advances 9 (2021) 100133.

[29] A. Rosenkranz, M.C. Righi, A.V. Sumant, B. Anasori, V.N. Mochalin, Perspectives of 2D MXene Tribology, Advanced Materials 35(5) (2023) 2207757.
[30] Y. Liu, X. Zhang, S. Dong, Z. Ye, Y. Wei, Synthesis and tribological property of Ti3C2TXnanosheets, Journal of Materials Science 52(4) (2017) 2200-2209.
[31] A. Rosenkranz, P.G. Grützmacher, R. Espinoza, V.M. Fuenzalida, E. Blanco, N. Escalona, F.J. Gracia, R. Villarroel, L. Guo, R. Kang, F. Mücklich, S. Suarez, Z. Zhang, Multi-layer Ti3C2Tx-nanoparticles (MXenes) as solid lubricants – Role of surface terminations and intercalated water, Applied Surface Science 494 (2019) 13-21.
[32] H. Zhang, L. Wang, Q. Chen, P. Li, A. Zhou, X. Cao, Q. Hu, Preparation, mechanical and anti-friction performance of MXene/polymer composites, Materials & Design 92 (2016) 682-689.
[33] B.C. Wyatt, A. Rosenkranz, B. Anasori, 2D MXenes: Tunable Mechanical and Tribological Properties, Advanced Materials 33(17) (2021) 2007973.
[34] X. Yin, H. Chen, L. Jiang, C. Liang, H. Pang, D. Liu, B. Zhang, Effects of polyacrylic acid molecular weights on V2C-MXene nanocoatings for obtaining ultralow friction and ultralow wear in an ambient working environment, Physical Chemistry Chemical Physics 24(44) (2022) 27406-27412.
[35] T.-S. Wong, S.H. Kang, S.K.Y. Tang, E.J. Smythe, B.D. Hatton, A. Grinthal, J. Aizenberg, Bioinspired self-repairing slippery surfaces with pressure-stable omniphobicity, Nature 477(7365) (2011) 443-447.
[36] Y. Li, L. Li, J. Sun, Bioinspired Self-Healing Superhydrophobic Coatings, Angewandte Chemie International Edition 49(35) (2010) 6129-6133.
[37] B.J. Blaiszik, S.L.B. Kramer, M.E. Grady, D.A. McIlroy, J.S. Moore, N.R. Sottos, S.R. White, Autonomic Restoration of Electrical Conductivity, Advanced Materials 24(3) (2012) 398-401.
[38] E. Palleau, S. Reece, S.C. Desai, M.E. Smith, M.D. Dickey, Self-Healing Stretchable Wires for Reconfigurable Circuit Wiring and 3D Microfluidics, Advanced Materials 25(11) (2013) 1589-1592.
[39] V. Presser, M. Naguib, L. Chaput, A. Togo, G. Hug, M.W. Barsoum, First-order Raman scattering of the MAX phases: Ti2AlN, Ti2AlC0.5N0.5, Ti2AlC, (Ti0.5V0.5)2AlC, V2AlC, Ti3AlC2, and Ti3GeC2, Journal of Raman Spectroscopy 43(1) (2012) 168-172.
[40] A. Sarycheva, T. Makaryan, K. Maleski, E. Satheeshkumar, A. Melikyan, H. Minassian, M. Yoshimura, Y. Gogotsi, Two-Dimensional Titanium Carbide (MXene) as Surface-Enhanced Raman Scattering Substrate, The Journal of Physical Chemistry C 121(36) (2017) 19983-19988.
[41] W.Y. Chen, X. Jiang, S.-N. Lai, D. Peroulis, L. Stanciu, Nanohybrids of a MXene and transition metal dichalcogenide for selective detection of volatile organic compounds, Nature Communications 11(1) (2020) 1302.
[42] J. Halim, K.M. Cook, M. Naguib, P. Eklund, Y. Gogotsi, J. Rosen, M.W. Barsoum, X-ray photoelectron spectroscopy of select multi-layered transition metal carbides (MXenes), Applied Surface Science 362 (2016) 406-417.
[43] C.E. Shuck, A. Sarycheva, M. Anayee, A. Levitt, Y. Zhu, S. Uzun, V. Balitskiy, V. Zahorodna, O. Gogotsi, Y. Gogotsi, Scalable Synthesis of Ti3C2Tx MXene, Advanced Engineering Materials 22(3) (2020) 1901241.
[44] A. Wollbrink, C.H. Rüscher, K. Volgmann, J. Koch, A. Breuksch, C. Tegenkamp, J. Caro, Improved hydrogen selectivity of Surface Modified Graphite (SMG) membranes: Permeation experiments and characterisation by micro-Raman spectroscopy and XPS, Journal of Membrane Science 528 (2017) 316-325.
[45] A. Ashraf, S.A. Dastgheib, G. Mensing, M.A. Shannon, Surface characteristics of selected carbon materials exposed to supercritical water, The Journal of Supercritical Fluids 76 (2013) 32-40.
[46] N. Dwivedi, R.J. Yeo, C. Dhand, J. Risan, R. Nay, S. Tripathy, S. Rajauria, M.S.M. Saifullah, S.K.R.S. Sankaranarayanan, H. Yang, A. Danner, C.S. Bhatia, Boosting contact sliding and wear protection via atomic intermixing and tailoring of nanoscale interfaces, Science Advances 5(1) eaau7886.
[47] T.S. Mathis, K. Maleski, A. Goad, A. Sarycheva, M. Anayee, A.C. Foucher, K. Hantanasirisakul, C.E. Shuck, E.A. Stach, Y. Gogotsi, Modified MAX Phase Synthesis for Environmentally Stable and Highly Conductive Ti3C2 MXene, ACS Nano 15(4) (2021) 6420-6429.

[48] S.A. Chambers, M.H. Engelhard, L. Wang, T.C. Droubay, M.E. Bowden, M.J. Wahila, N.F. Quackenbush, L.F.J. Piper, T.-L. Lee, C.J. Nelin, P.S. Bagus, X-ray photoelectron spectra for single-crystal $\mathrm{T}{\mathrm{i}}_{2}{\mathrm{O}}_{3}$: Experiment and theory, Physical Review B 96(20) (2017) 205143.
[49] J.E. von Treifeldt, K.L. Firestein, J.F.S. Fernando, C. Zhang, D.P. Siriwardena, C.-E.M. Lewis, D.V. Golberg, The effect of Ti3AlC2 MAX phase synthetic history on the structure and electrochemical properties of resultant Ti3C2 MXenes, Materials & Design 199 (2021) 109403.
[50] S. Jaiswal, J. Vishwakarma, S. Bhatt, S. Karak, P. Bharti, C. Dhand, R. Kumar, P. Kumar, M.S.M. Saifullah, S. Saha, R. Mishra, N. Dwivedi, Layered Titanium Carbide-Mediated Fast Shape Switching and Excellent Thermal and Electrical Transport in Shape-Memory-Polymer Composites for Smart Technologies: MAX Versus MXene, Advanced Engineering Materials n/a(n/a) (2023) 2300233.
[51] Y. He, Z. Zhang, Y. Wang, M. Liu, C. Liao, J. Yuan, P. Li, M. Yang, W. Liu, Synergistic effects of bioprotein decoration and WS2 @Ti3C2 nanohybrids on the interfacial and tribological performance of PPS/PTFE fabric composites, Tribology International 186 (2023) 108587.
[52] S. Li, C. Dong, C. Yuan, X. Bai, Friction-reducing and vibration-absorbing performances on a novel thermoplastic bearing material reinforced by nano-WS2 and UHMWPE, Tribology International 176 (2022) 107893.
[53] D. Simić, D.B. Stojanović, A. Kojović, M. Dimić, L. Totovski, P.S. Uskoković, R. Aleksić, Inorganic fullerene-like IF-WS2/PVB nanocomposites of improved thermo-mechanical and tribological properties, Materials Chemistry and Physics 184 (2016) 335-344.
[54] B. Chen, Y. Jia, M. Zhang, H. Liang, X. Li, J. Yang, F. Yan, C. Li, Tribological properties of epoxy lubricating composite coatings reinforced with core-shell structure of CNF/MoS2 hybrid, Composites Part A: Applied Science and Manufacturing 122 (2019) 85-95.
[55] L. Xu, Y. Zheng, Z. Yan, W. Zhang, J. Shi, F. Zhou, X. Zhang, J. Wang, J. Zhang, B. Liu, Preparation, tribological properties and biocompatibility of fluorinated graphene/ultrahigh molecular weight polyethylene composite materials, Applied Surface Science 370 (2016) 201-208.
[56] G. Ren, Z. Zhang, X. Zhu, B. Ge, F. Guo, X. Men, W. Liu, Influence of functional graphene as filler on the tribological behaviors of Nomex fabric/phenolic composite, Composites Part A: Applied Science and Manufacturing 49 (2013) 157-164.
[57] X. Ao, D. Kong, Z. Zhang, X. Xiao, Enhancing recovery speed and anti-wear capability of high-temperature shape memory polymer with modified boron nitride nanoparticles, Journal of Materials Science 55(10) (2020) 4292-4302.
[58] S.S. El-Deen, A.M. Hashem, A.E. Abdel Ghany, S. Indris, H. Ehrenberg, A. Mauger, C.M. Julien, Anatase TiO2 nanoparticles for lithium-ion batteries, Ionics 24(10) (2018) 2925-2934.
[59] P. Xue, Z. Huang, C. Chen, Effect of Substrate Roughness on the Friction and Wear Behaviors of Laser-Induced Graphene Film, Lubricants 10(10) (2022) 239.
[60] L. Chang, Z. Zhang, C. Breidt, K. Friedrich, Tribological properties of epoxy nanocomposites: I. Enhancement of the wear resistance by nano-TiO2 particles, Wear 258(1) (2005) 141-148.
[61] E. Marquis, M. Cutini, B. Anasori, A. Rosenkranz, M.C. Righi, Nanoscale MXene Interlayer and Substrate Adhesion for Lubrication: A Density Functional Theory Study, ACS Applied Nano Materials 5(8) (2022) 10516-10527.
[62] M.W. Barsoum, The MN+1AXN phases: A new class of solids: Thermodynamically stable nanolaminates, Progress in Solid State Chemistry 28(1) (2000) 201-281.
[63] M.W. Barsoum, M. Radovic, Elastic and Mechanical Properties of the MAX Phases, Annual Review of Materials Research 41(1) (2011) 195-227.